

Identification of potential crucial genes associated with vasculogenic mimicry in human osteosarcoma based on gene expression profile

N. YAO^{1,2*}, K. REN^{3,*}, X. J. GU⁴, S. J. WU⁵, X. SHI⁵, Q. CHANG³, Y.G. LI³, Z. X. GAO³, Q. M. JIN^{1,2}, J. ZHANG^{1,2}, C. WANG^{3,*}, J. ZHOU^{1,2,6*}

¹Affiliated Hospital of Integrated Traditional Chinese and Western Medicine, Nanjing University of Chinese Medicine, Nanjing 210028, Jiangsu, China; ²Laboratory of Translational Medicine, Jiangsu Province Academy of Traditional Chinese Medicine, Nanjing 210028, Jiangsu, China; ³Department of Orthopedics, Zhongda Hospital, Southeast University, Nanjing, 210009, Jiangsu, China; ⁴Institute of Biotechnology, School of Environmental and Chemical Engineering, Dalian Jiaotong University, Dalian 116028, Liaoning, China; ⁵Department of Orthopedics, Jinling Hospital, Nanjing University, School of Medicine, Nanjing 210002, Jiangsu Province, China; ⁶School of Basic Medicine and Clinical Pharmacy, China Pharmaceutical University, Nanjing 211198, Jiangsu Province, China

*Correspondence: chenwang_southeast@126.com; happyjingzhou@126.com

*Contributed equally to the work.

Received April 14, 2019 / Accepted July 9, 2019

We previously reported the presence of vasculogenic mimicry (VM) in human osteosarcoma. However, the mechanistic basis of osteosarcoma VM remains unclear. Three hundred eighty-one upregulated differentially expressed genes (DEGs) and 526 downregulated DEGs between human osteosarcoma cell line 143B and HOS cell exposed to Matrigel were screened out by microarray. GO categories such as “cell adhesion”, “angiogenesis” were enriched in 143B group. PATHWAY analysis showed enriched TGF- β , Wnt and VEGF signaling pathway in 143B group. The hub gene ITGA2 in signal-network of DEGs exhibited pro-VM and pro-metastasis effect. Our study provides fundamental data for further studies regarding molecules involved in osteosarcoma VM.

Key words: osteosarcoma, microarray analysis, neoplasm metastasis

In 1999, Maniotis et al. [1] first reported a novel phenomenon in tumor angiogenesis: vasculogenic mimicry (VM). It describes functional plasticity of highly aggressive and invasive tumor cells in dedifferentiating to a vascular phenotype and forming *de novo* tube-like networks, thus distributing red blood cells and nutrition to malignant tumor growth independent of conventional vasculogenesis or angiogenesis. It also provides a unique structure in which the inner surface of the networks exposes tumor cells direct to the blood stream, thus greatly promoting tumor metastasis to distant sites [2]. These tubular networks could also be observed *in vitro* with highly invasive tumor cells in three-dimensional culture conditions, which comprised of extracellular matrix (ECM) and resemblances with tube-like structures observed in classic endothelial cell-based *in vitro* angiogenesis assay [3].

Since its first report in melanoma, VM has been involved in a variety of malignant human tumors including osteosarcoma [4]. VM is associated with poor clinical outcome, reduced patient survival and increased risk of metastasis [2]. These findings were consistent with our previous report

that in patients with osteosarcoma, VM is associated with decreased overall survival rates and the development of distant metastasis, thus serving as an unfavorable prognostic factor for osteosarcoma patients [4]. Similarly, there is a correlation between the histological detection of VM in *in vivo* osteosarcoma xenograft model and subsequent death from metastasis, in accordance with the *in vitro* observations showing that VM channels are formed by highly invasive osteosarcoma cells [5, 6].

Microarray studies comparing VM-positive aggressive tumor cells and non-VM tumor cells revealed multiple signaling molecules and cascades involved in VM. For example, VE-cadherin and EPHA2 are two of the first molecules identified to play a key role in mediating VM [7]. Other molecules including Galectin-3, cAMP, COX-2 and MIG-7 have been reported to be engaged in VM [8]. Signaling pathway like HIF-1 α , Notch/Nodal and Wnt/ β -catenin were shown to contribute to VM formation [8]. Targeting VM with specific compounds may become a promising therapeutic approach against tumor progression [9]. However, the mechanism of osteosarcoma VM remains unclear since its

first report in 2004. It is therefore of extreme importance and urgent demand to explore the molecules underlying osteosarcoma VM to define potential genetic targets for therapeutic development against osteosarcoma.

It is well known that microarray-based gene expression profiling studies in cancer provide a high-throughput, efficient approach to gain a wealth of information with potential diagnostic and prognostic uses and to investigate the mechanisms that underscore tumorigenic phenotype. Because VM formation requires tumor cells cultured in an ECM-rich microenvironment, we herein compared gene expression profiles between commonly used human metastatic 143B osteosarcoma cell line and non-metastatic HOS osteosarcoma cell line in three dimensional Matrigel matrices for two reasons: firstly, 143B cells could form VM channels on Matrigel, an ECM extract culture medium used for *in vitro* tube formation assay [5], whereas HOS cells could not (Figure 1). Secondly, as many human osteosarcoma cell lines are derived from different genetic origins, we therefore applied commonly used human metastatic osteosarcoma cell line 143B and its parental non-metastatic lines HOS to avoid interference from different genetic background.

In the present study, we performed gene expression profiling to identify differentially expressed genes (DEGs) between 143B cells and HOS cells cultured on Matrigel to fully understand VM phenotypes at the molecular level. Then, we analyzed their functions by GSEA GO analysis and GSEA pathway analysis. Signal network (Signal-net) was conducted to show hub genes that might play critical roles in osteosarcoma VM formation. Finally, we demonstrated a top-ranked hub gene *ITGA2* had a VM-promoting role in osteosarcoma. This study aimed to shed light on the molecular underpinnings of osteosarcoma VM, and clarify novel therapeutic targets for the development of innovative treatment strategies for osteosarcoma.

Materials and methods

Cell lines and culture. Human osteosarcoma cells (HOS and 143B) were purchased from the American Type Culture Collection (ATCC, Manassas, VA, USA) and cultivated, according to the recommendation of the supplier, in RPMI 1640 (Invitrogen, Carlsbad, CA, U.S.) containing 10% FBS (Gibco Life Technologies, Grand Island, NY, U.S.) and DMEM (Invitrogen) containing 10% FBS, respectively. Streptomycin (100 mg/ml) and penicillin (100 U/ml) were added to each medium. All cells were cultured in T75 flasks (Nunc, U.S.) in a humidified incubator at 37°C with 5% CO₂, and culture medium exchange was performed every 24 hours.

VM assay. A 6-well plate was evenly coated with 1 ml/well cold Matrigel (BD Biosciences, San Jose, CA, USA, thawed at 4°C) and allowed to solidify at 37°C for 30 min. Then cell suspension (6×10⁵/ml) was added (1 ml/well) onto the surface of the plate and incubated at 37°C for 3, 8, 12 and

24 h, respectively. Cells were photographed under a light microscope (Primo Vert, Zeiss, Germany).

RNA preparation. Twenty-four hours after osteosarcoma cell lines were seeded on Matrigel, total RNA was extracted using Trizol reagent (Invitrogen, Carlsbad, CA, U.S.) according to the manufacturer's instructions. RNA integrity was assessed by electrophoresis on a denaturing agarose gel. RNA concentration and purity were determined by a NanoDrop 2000 spectrophotometer using OD₂₆₀ and OD₂₆₀/OD₂₈₀ ratio, respectively. The extracted RNA samples were stored at -80°C for further experiments.

Microarray assay. Global gene expression profiling analysis was performed using Affymetrix GeneChip® Human Transcriptome 2.0 Array (HTA2.0, Affymetrix, Santa Clara, CA, USA). Briefly, 250 ng total RNA was reverse transcribed to biotinylated cDNA using GeneChip® WT PLUS Reagent Kit according to the standard Affymetrix protocol. Following labeling, cDNA was hybridized for 16 h at 45°C on GeneChip Human Transcriptome Array 2.0 in GeneChip® Hybridization Oven 645 (Affymetrix). GeneChips were washed and stained in the Affymetrix Fluidics Station 450, and then scanned using the Hewlett-Packard GeneArray Scanner 3000 7G. Data was submitted to the Gene Expression Omnibus (GEO) repository (<https://www.ncbi.nlm.nih.gov/geo/>) with accession number GSE119975 (GEO: GSE119975).

Data preprocessing and DEG identification. The data were analyzed with Robust Multichip Analysis (RMA) algorithm using Affymetrix default analysis settings and global scaling as normalization method. The DEGs between HOS and 143B cells were screened out using the cut-off criteria of fold change (FC) ≥3.0 and p-value <0.05.

Clustering analysis of DEGs. Hierarchical clustering of DEGs based on the Euclidean distance was built using the R heatmap package (cran.r-project.org/web/packages/heatmap/index.html) and the heat map results were visualized using Heatmap software (version 1.0, <https://www.hiv-lanl.gov.vpn.seu.edu.cn/content/sequence/HEATMAP/heatmap.html>).

GSEA analysis. GSEA is a computational approach to identify classes of genes that are over-represented in a large set of genes between two biological states, such as disease phenotypes. GSEA software version 2.2.3 and gene sets obtained from Molecular Signatures Database v5.1 (MsigDB) (<http://software.broadinstitute.org/gsea/index.jsp>) or from published gene signatures were used for analysis. GSEA starts with a list of genes ranked by using a signal-to-noise metric and according to their differential expression levels across HOS and 143B group. Then enrichment score was calculated based on a weighted Kolmogorov-Smirnov-like statistic. Statistical significance was assessed by comparing the enrichment score to enrichment results generated from 1,000 random permutations of the gene set to obtain p-values (nominal p-value). The significant threshold was set at p-value <0.01 in this study.

Signal-net analysis. Signal-net analysis of DEGs was built based on KEGG database to illustrate gene regulatory network. Networks were presented as graphs, where nodes are mainly genes and edges represent relation types between the nodes, such as activation or inhibition. Degree centrality is an index that weighs the importance of a certain gene, including indegree and outdegree. The degree of a node is defined as the number of links between this node itself and all other nodes. Gene with higher degrees implies a greater ability to modulate genes those it correlates with.

qPCR. A total of 1 μg RNA used as template was reverse transcribed to first-strand cDNA using a HiScript[®] II QRT SuperMix for qPCR (Vazyme Biotech Co., Ltd., Nanjing, China). Quantitative PCR was performed in total reaction volume of 20 μl using ChamQ[™] Universal SYBR[®] qPCR Master Mix (Vazyme). The primers were synthesized by Genaray Corporation (Shanghai, China). The sequence of primers was shown in Table S1. The qPCR assays were performed using the QuantStudio Dx instrument (Life Technologies, Foster City, CA). GAPDH was chosen as the endogenous standard. Expression level of individual gene was normalized to GAPDH according to the $2^{-\Delta\Delta\text{CT}}$ method.

Western blot. Cells were washed twice with PBS and lysed in lysis buffer at 4 °C. Equal amounts of protein (30 μg) were separated by SDS-PAGE and transferred to PVDF membranes. The membrane was incubated with anti-ITGA2 antibody (R&D systems) and detected by using a DyLight secondary antibody (CST, MA, USA). ITGA2 protein expression was normalized against β -Actin.

siRNA transfection. The small interfering RNAs (siRNA) targeting *ITGA2* were purchased from Thermo Fisher Scientific (Carlsbad, CA). The sequences of siRNA were as follows: si*ITGA2*#1: 5'-GACCAUUGUCCAGAAGACAUCUCAU-3', si*ITGA2*#2: 5'-GCCUGCAGAAGAAUAUGGUAGUAAA-3', and a none-related control siRNA (Invitrogen#12935300) was used as a negative control. Transfections were performed in 143B cells using the Lipofectamine RNAiMAX Reagent (Invitrogen) according to the manufacturer's instructions. The knockdown efficiency was verified 24 h after transfection.

Lentivirus shRNA knockdown of *ITGA2*. The *ITGA2* shRNA (sequences: 5'-ATGGCAATATCACGGTTATTC-3') or one off-target shRNA (sequences: 5'-TTCTCCGAACGTGTCACGT-3') in the lentiviral expression vector pLenR-GPH was purchased from Nanjing KeyGen Biotech Co., Ltd. (Nanjing, China). Then the recombinant lentivirus was produced by co-transfecting 293FT cells with packaging helper plasmids and pLenR-GPH-*ITGA2* shRNA or pLenR-GPH-NC shRNA vectors. 143B cells transduced with lentivirus *ITGA2* shRNA vector or lentivirus shRNA control vector are designated as *ITGA2* KD or NC cells. The knockdown of *ITGA2* was evaluated by qPCR and Western blot.

In vivo tumor xenograft model. The Institutional Animal Care and Use Committee (IACUC) of the Jiangsu Province

Academy of Traditional Chinese Medicine approved the animal study that was conducted in accordance with the National Institutes of Health Guide for the Care and Use of Laboratory animals. Six-week-old male BALB/C nude mice, purchased from Shanghai lingchang Bio-Tech Co., Ltd. (Certificate no. SCXK (HU) 2017-0005), were intratibially injected with 5×10^5 NC or *ITGA2* KD 143B cells in 10 μl of PBS. Each group contained eight mice. Tumor volume (V) was measured every 3 days by gauging the length (L) and width (W) of the cell-injected and the healthy control right leg with calipers ($V = V_{\text{left leg}} - V_{\text{right leg}}$, leg volume [mm^3] = $0.5 \times L \times W^2$). Mice were sacrificed 30 days after injection and the primary tumors and lungs were harvested. Lung metastasis was quantified by counting the number of tumor nodule on lung surface with stereomicroscope (Stemi 2000-C, Zeiss, Germany). Organs were then fixed in formaldehyde for further examination.

Histology analysis. Tumor and lung samples were embedded in paraffin, sectioned (4 μm), and stained with Hematoxylin and eosin (H&E) for general histopathology.

Immunohistochemical analysis and quantification. Paraffin sections were deparaffinized by xylene and rehydrated in decreasing concentrations of ethanol. After blocking endogenous peroxidase with 3% hydrogen peroxidase in methanol for 10 min at room temperature, sections were boiled on citrate buffer for 10 min and incubated with 10% normal blocking serum for 20 min. The sections were then incubated with anti-ITGA2 antibody (R&D systems) overnight at 4 °C, followed by immunodetection using the Envision System (DAKO, Glostrup, Denmark). The slides were then counterstained with hematoxylin for 1 min and mounted. For quantification, the expression level of ITGA2 was scored using a composite score by combining the percentage of positively stained tumor cells and the intensity of staining [10]. The percentage of positive cells was scored as: 0, no positive tumor cells; 1, <10%; 2, 10–35%; 3, 35–75%; 4, >75%. The intensity of staining was scored as: 0, no or weak staining (light yellow); 1, moderate staining (yellow brown); 2, strong staining (brown).

CD31/PAS double immunohistochemical staining was performed to detect the presence of VM as we previously described [5]. For quantification, VM density (VMD) was defined as the average VM count from five $\times 400$ magnification fields per slide. The average VMD from eight tumor samples was obtained as the final VMD count.

Statistical analysis. Results were expressed as the mean \pm S.D. The random variance model (RVM) t was used for detection of the differentially expressed genes for the 143B and HOS groups. The one-way ANOVA test was used to compare quantitative data. A value of false discovery rate (FDR) or p-value less than 0.05 was considered statistically significant.

Data availability. The microarray data are publicly available in the GEO repository under accession number GSE119975 (GEO: GSE119975).

Results

Chronological changes of VM formation by osteosarcoma cells. A tube formation assay using Matrigel composed of ECM has been used to test the ability of tumor cells to develop a vascular phenotype, also known as VM. As shown in Figure 1, after 3 h the highly aggressive 143B cells on Matrigel orientated themselves towards each other and began to build up cell-to-cell links. The tubular channels developed dynamically and inosculated during an 8 to 24 h period. These networks consisted of clear elongated cell bodies, which formed polygonal-shape meshwork. At 24 h, complete tubular networks have virtually established and seldom-isolated cells were left out. In contrast, the lowly invasive HOS cells failed to develop tubular networks on Matrigel at any time point. In this Matrigel-based culture system, HOS cells exhibited the feature of small, round colony morphology (Figure 1). Evidence demonstrated that this assay should be finished within 24 h because the cells commonly undergo cell death after 24 h, leading to tube detachment and disruption [11]. Therefore, we chose a time point of 24 h for subsequent study when VM formation is mature but discontinued network is not obvious.

Identification of DEGs between 143B and HOS group. Based on the cut-off criteria, a total of 907 DEGs were identified between the 143B and HOS groups, of which 381 were upregulated in 143B compared with HOS group and 526 were downregulated. Among these DEGs, *MMP1* (matrix metalloproteinase 1) was the most upregulated, with an FC of 1273.01, whereas *MYL9* (myosin, light chain 9, regulatory) was the most downregulated, FC being 178.57. The top 10 upregulated and downregulated DEGs are listed in Table 1. A hierarchical clustering analysis heatmap presented in Figure 2 showed a clear distinction between 143B and HOS groups.

GSEA GO analysis. To investigate underlying mechanisms involved in the VM, we used GSEA to identify gene

sets and key pathways that are altered in 143B and HOS groups. The results of the GO analysis based on normalized enriched score (NES) and p-value (<0.01) are shown for 143B and HOS groups in Tables 2, 3 and Figure S1A, S1B. We identified GO categories including “cell adhesion”, “angiogenesis”, “positive regulation vascular endothelial growth factor production”, “positive regulation of Wnt receptor signaling pathway”, “positive regulation of endothelial cell proliferation” and “regulation of transforming growth factor beta

Table 1. The top 10 significant upregulated and downregulated DEGs in 143B versus HOS groups.

Probe set	Gene symbol	Fold change	p-value
Upregulated			
TC11002234.hg.1	<i>MMP1</i>	1273.01	<10 ⁻⁷
TC05000218.hg.1	<i>ITGA2</i>	417.67	<10 ⁻⁷
TC08001321.hg.1	<i>TRPA1</i>	133.84	<10 ⁻⁷
TC01003042.hg.1	<i>TBX15</i>	121.19	<10 ⁻⁷
TC15001837.hg.1	<i>ANPEP</i>	67.33	<10 ⁻⁷
TC0X000954.hg.1	<i>SRPX</i>	66.83	<10 ⁻⁷
TC04002931.hg.1	<i>PDGFRA</i>	46.54	<10 ⁻⁷
TC09001278.hg.1	<i>FRMD3</i>	43.01	<10 ⁻⁷
TC02002098.hg.1	<i>LOC100996862</i>	38.33	<10 ⁻⁷
TC05000372.hg.1	<i>F2RL1</i>	37.42	<10 ⁻⁷
Downregulated			
TC20000268.hg.1	<i>MYL9</i>	178.57	<10 ⁻⁷
TC08001051.hg.1	<i>TNFRSF10D</i>	40.00	<10 ⁻⁷
TC10000771.hg.1	<i>INA</i>	37.04	<10 ⁻⁷
TC17000309.hg.1	<i>WSB1</i>	29.41	<10 ⁻⁷
TC10000415.hg.1	<i>SRGN</i>	29.41	<10 ⁻⁷
TC06001271.hg.1	<i>ELOVL2</i>	28.57	<10 ⁻⁷
TC01003796.hg.1	<i>SLC30A1</i>	27.78	<10 ⁻⁷
TC0X000195.hg.1	<i>USP9X</i>	20.83	<10 ⁻⁷
TC06000640.hg.1	<i>CENPQ</i>	18.87	<10 ⁻⁷
TC06001782.hg.1	<i>MUT</i>	18.52	<10 ⁻⁷

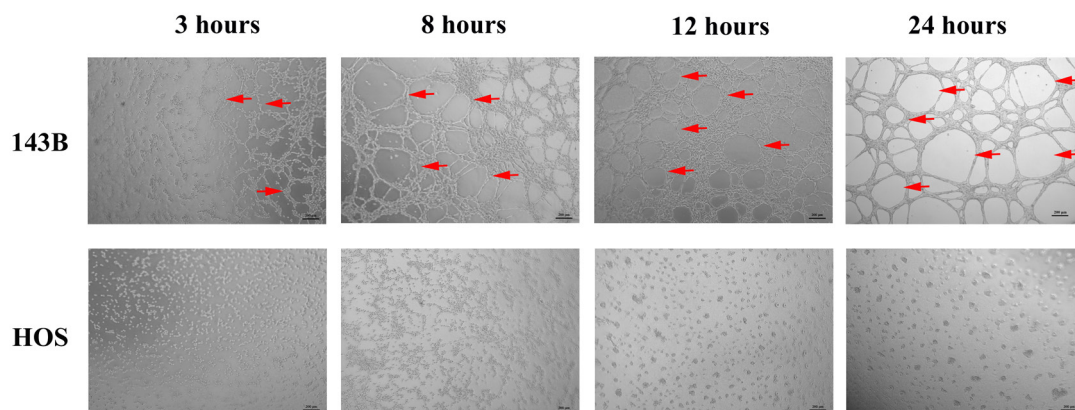


Figure 1. Kinetics of VM formation by osteosarcoma cells. Cells were plated on Matrigel and images were taken at different times indicated. 143B cells started to form VM channels as early as 3 hours after plating on Matrigel. Well-defined capillary-like tubes were observed by 24 hours. HOS cells failed to form patterned networks. Scale bar: 200 μ m; arrows denote VMs formed by 143B cells.

receptor signaling pathway” were enriched in 143B groups, suggesting blood vessel development and tumor progression involved in 143B groups. In HOS groups, GO categories such as “collagen fibril organization”, “keratinocyte differentiation”, “glycosaminoglycan biosynthetic process” were enriched, suggesting a matrix-producing phenotype in HOS cells.

GSEA PATHWAY analysis. The results of the pathway analysis based on normalized enrichment score (NES) and p-value (<0.01) are shown for 143B and HOS groups in Tables 4, 5 and Figure S1C, S1D. We identified pathways involved in tumor development and angiogenesis such as “TGF-beta signaling pathway”, “Wnt signaling pathway”, “VEGF signaling pathway” and “Chemical carcinogenesis” were significantly upregulated in 143B group. In HOS group, pathways including “Type II diabetes mellitus” and “Amoebiasis” were upregulated.

Signal-net analysis. Gene signal transduction networks (Signal-net) was performed to clarify the key genes involved in VM formation in osteosarcoma. As shown in Figure 3, there was a mount of 47 key genes, which were obtained in the Signal-net. As shown in Table 6, the top 10 genes ranked according to degree value were *ITGA2* (integrin subunit alpha 2), *PRKACB* (protein kinase cAMP-activated catalytic subunit beta), *ITGA1* (integrin subunit alpha 1), *ITGA6* (integrin subunit alpha 6), *ACTN1* (actinin alpha 1), *ACTN4* (actinin alpha 4), *PLCB4* (phospholipase C beta 4), *PDGFRB* (platelet derived growth factor receptor beta), *PDGFRA* (platelet derived growth factor receptor alpha), *GJA1* (gap junction protein alpha 1).

qRT-PCR validation. To validate the accuracy of the microarray, we chose a total of 14 DEGs including top five upregulated genes (*MMP1*, *ITGA2*, *TRPA1*, *TBX15*, *ANPEP*),

Table 2. Gene sets enriched in 143B group.

Gene Set ID	Gene Set Name	Size	NES	NOM p-val	FDR q-val
GO_0007155	cell adhesion	72	2.24	0	0.02
GO_0001525	angiogenesis	45	2.09	0.0020	0.06
GO_0010575	positive regulation vascular endothelial growth factor production	6	2.07	0	0.06
GO_0030177	positive regulation of Wnt receptor signaling pathway	6	1.91	0.0020	0.14
GO_0001938	positive regulation of endothelial cell proliferation	9	1.89	0.0059	0.15
GO_0017015	regulation of transforming growth factor beta receptor signaling pathway	6	1.84	0.0043	0.21

NES, normalized enrichment score; NOM p-value, nominal p value; FDR q-val, false discovery rate q value.

Table 3. Gene sets enriched in HOS group.

Gene Set ID	Gene Set Name	Size	NES	NOM p-val	FDR q-val
GO_0030199	collagen fibril organization	12	-2.59	0	0.00
GO_0030216	keratinocyte differentiation	10	-1.96	0	0.35
GO_0043434	response to peptide hormone stimulus	10	-1.96	0.0040	0.24
GO_0006024	glycosaminoglycan biosynthetic process	6	-1.95	0	0.20
GO_0070509	calcium ion import	4	-1.89	0	0.29

NES, normalized enrichment score; NOM p-value, nominal p value; FDR q-val, false discovery rate q value.

Table 4. Signaling pathways enriched in 143B group.

Gene Set ID	Gene Set Name	Size	NES	NOM p-val	FDR q-val
PATH4350	TGF-beta signaling pathway	16	2.19	0	0.02
PATH4310	Wnt signaling pathway	21	2.08	0.0020	0.03
PATH4370	VEGF signaling pathway	8	1.96	0.0020	0.06
PATH5204	Chemical carcinogenesis	3	1.67	0.0082	0.22

NES, normalized enrichment score; NOM p-value, nominal p value; FDR q-val, false discovery rate q value.

Table 5. Signaling pathways enriched in HOS group.

Gene Set ID	Gene Set Name	Size	NES	NOM p-val	FDR q-val
PATH5146	Amoebiasis	20	-1.84	0.0060	0.70
PATH4930	Type II diabetes mellitus	3	-1.71	0.0021	0.62

NES, normalized enrichment score; NOM p-value, nominal p value; FDR q-val, false discovery rate q value.

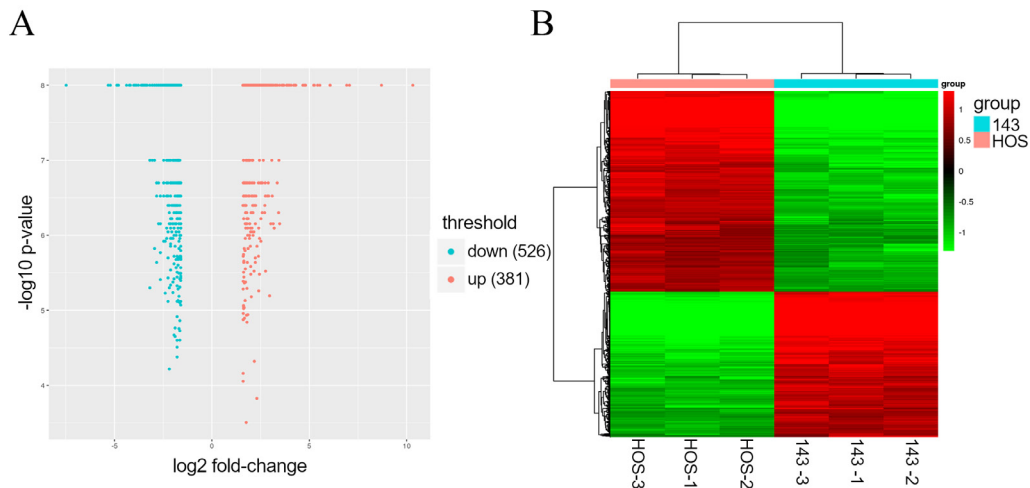


Figure 2. Microarray gene expression profiling of 143B vs. HOS groups. A) Volcano plot shows differentially expressed genes comparing 143B and HOS groups. Red dots represent genes overexpressed in 143B group (fold change ≥ 3 , p-value < 0.05). Blue dots represent genes underexpressed in 143B group (fold change ≥ 3 , p-value < 0.05). B) Hierarchical clustering analysis heat-map shows differentially expressed genes in 143B and HOS groups. Red represents upregulated genes and green represents downregulated genes.

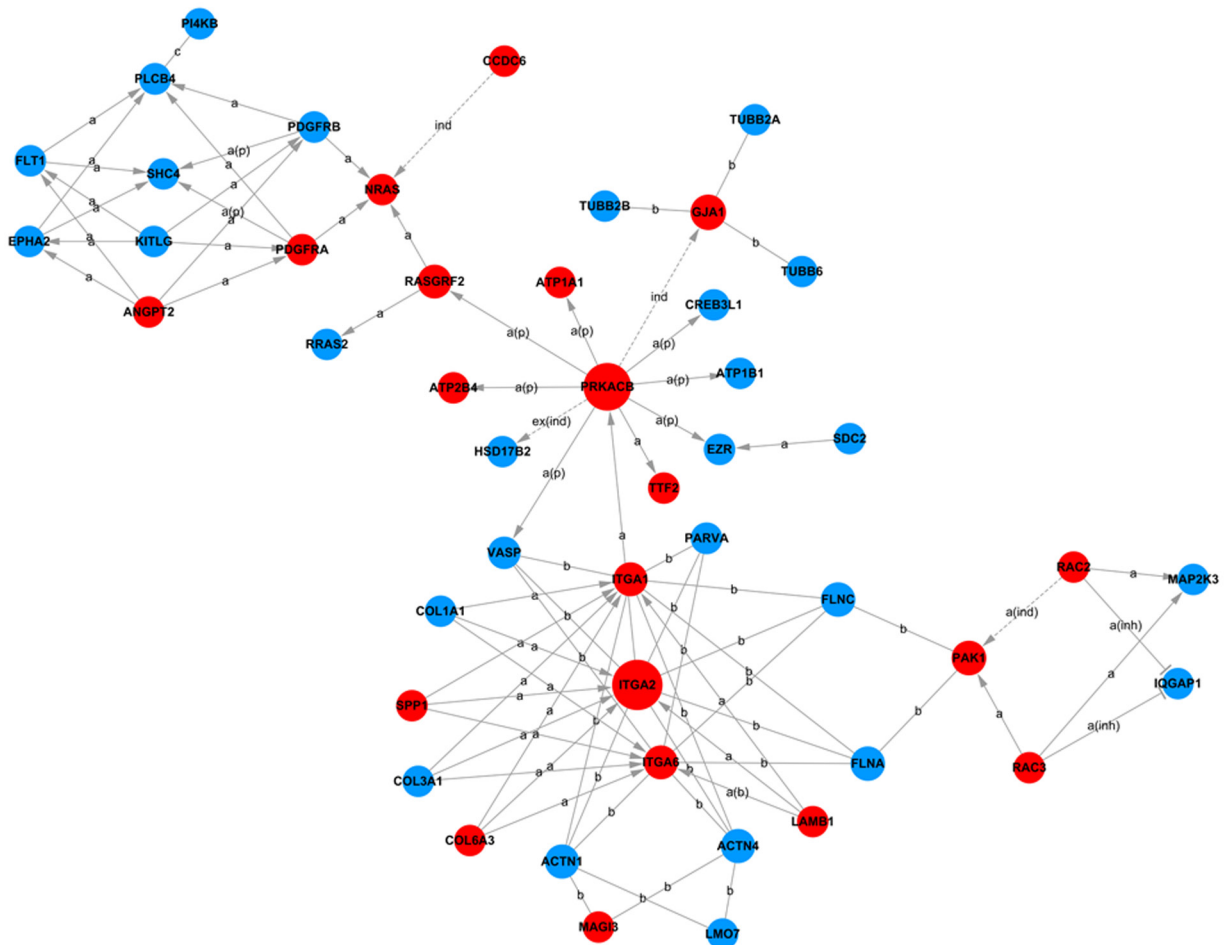


Figure 3. Signal-net analysis of DEGs. The red circle represents the upregulated DEGs and the blue circles downregulated DEGs. The area of the circle represents the betweenness centrality. Interaction between the genes is shown as a: activation, a(inh): activation (inhibition), a(b): activation (binding/association), a(p): activation (phosphorylation), b: binding/association, c: compound, ex(ind): expression (indirect effect), ind: indirect effect.

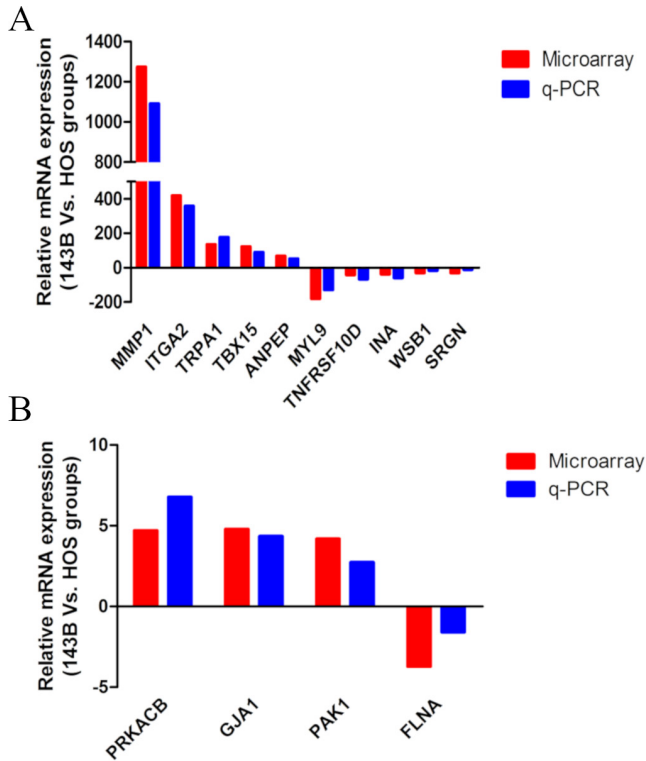


Figure 4. qRT-PCR of dysregulated mRNA shows the same regulation of mRNA with microarray results. A) Ten dysregulated mRNAs were chosen for being the top upregulated and downregulated mRNAs. B) Four dysregulated mRNAs were chosen for being the top four key genes identified in Signal-net analysis. * $p < 0.05$ for each mRNA.

Table 6. Top 10 DEGs identified by Signal-net analysis.

Gene symbol	Description	Degree	Indegree	Outdegree
<i>ITGA2</i>	integrin subunit alpha 2	12	11	7
<i>PRKACB</i>	protein kinase cAMP-activated catalytic subunit beta	11	1	10
<i>ITGA1</i>	integrin subunit alpha 1	11	11	6
<i>ITGA6</i>	integrin subunit alpha 6	11	11	6
<i>ACTN1</i>	actinin alpha 1	5	5	5
<i>ACTN4</i>	actinin alpha 4	5	5	5
<i>PLCB4</i>	phospholipase C beta 4	5	5	1
<i>PDGFRB</i>	platelet derived growth factor receptor beta	5	2	3
<i>PDGFRA</i>	platelet derived growth factor receptor alpha	5	2	3
<i>GJA1</i>	gap junction protein alpha 1	4	4	3

top five downregulated genes (*MYL9*, *TNFRSF10D*, *INA*, *WSB1*, *SRGN*) and four top key genes (*PRKACB*, *ITGA1*, *ITGA6*, *ACTN1*) identified in Signal-net analysis for qRT-PCR verification. Expression levels of these 14 DEGs were approximately consistent with the microarray results (Figure 4).

***ITGA2* knockdown inhibited VM formation by 143B cells *in vitro* and *in vivo*.** Hub genes are defined as a small ratio of nodes with the highest connectivity with other genes in the constructed gene network and often possess biological activity as well. We chose the top one hub gene *ITGA2*, which was also ranked second highest among upregulated DEGs to evaluate its role in osteosarcoma VM formation.

Firstly, we used siRNA to silence *ITGA2* to test its impact on *in vitro* VM in 143B cell lines. As shown in Figure 5A and 5B, two siRNAs significantly decreased the levels of *ITGA2* mRNA and protein in comparison with control cells transfected with negative control siRNA. Secondly, *in vitro* VM assay showed that a knockdown of *ITGA2* resulted in a significant decrease of VM channels in 143B cells (Figure 5C). To evaluate the effect of *ITGA2* knockdown *in vivo*, *ITGA2* KD 143B cells were intratibially inoculated in the left tibia of the nude mice. *ITGA2* KD group formed smaller tumors at 30 days post-implantation when compared to NC group (Figure 5D). Primary tumor growth was inhibited in *ITGA2* KD group compared to NC group during 30 days (Figure 5E). qPCR and immunohistochemical assays were performed to confirm the efficacy of *ITGA2* knockdown in tumor tissues. As anticipated, *ITGA2* KD group displayed reduced *ITGA2* expression (Figures 5F, 5H, 5I). Thirdly, *ITGA2* knockdown resulted in significant decreases in the number of lung metastatic nodules (Figures 5D, 5G). H&E staining of the primary tumors and lungs tissues showed more osteosarcoma cells with strongly stained enlarged nucleoli in *ITGA2* KD group than in NC group (Figure 5H). Tumors in *ITGA2* KD group showed reduced VMD compared with NC group (Figure 5J). Collectively, these data demonstrate that *ITGA2* knockdown can suppress osteosarcoma VM and metastasis.

Discussion

Osteosarcoma is the most frequent primary malignant bone tumor mainly affecting adolescents and children with a high propensity for fatal metastases. The 5-year survival rate of patients with localized osteosarcoma has increased from 20% to 70% due to the introduction of neo-adjuvant chemotherapy combined with increasingly improved surgical approaches [12]. However, patients with metastases, still have poor prognoses, with overall survival rates of approximately 20% [13]. Consequently, it is crucial to identify the mechanism of metastasis in osteosarcoma for more effective treatment. Due to VM's contribution to distant metastasis and poor clinical outcome, which we have previously reported [4], it is of great importance to dissect the molecules involved in mediating osteosarcoma VM.

To our knowledge, this study is the first attempt to provide a genome-wide transcriptional comparative analysis between VM-positive and VM-negative osteosarcoma cells. We obtained many DEGs between 143B and HOS groups, among which, several showed remarkable fold change such as *MMP1*, *ITGA2* and *MYL9*. Reports show that these DEGs

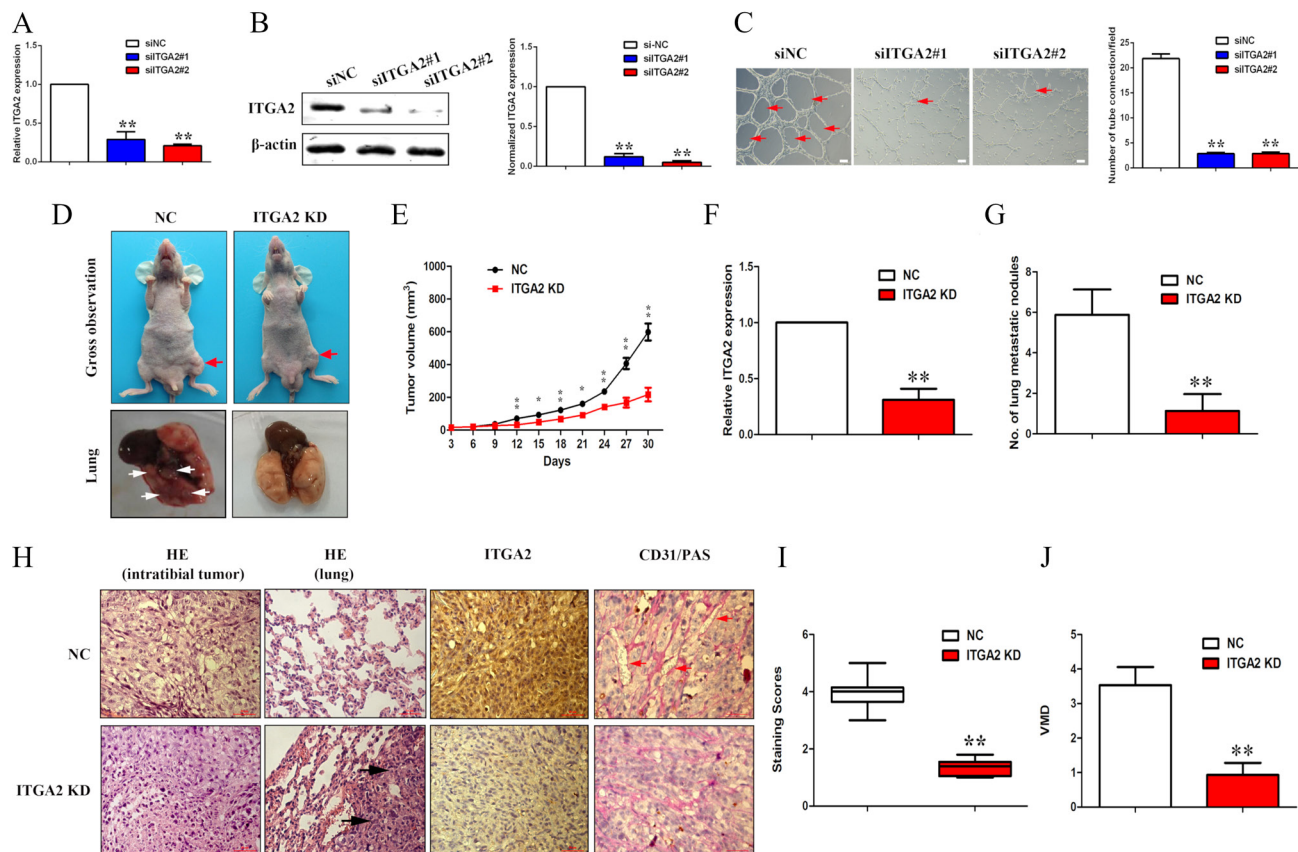


Figure 5. *ITGA2* knockdown inhibited osteosarcoma VM formation and metastasis. The mRNA and protein expression of *ITGA2* in *ITGA2*-knockdown 143B cells were detected using qRT-PCR (A) and western blot (B). C): *In vitro* VM formation in *ITGA2*-knockdown 143B cells was analyzed using Matrigel-based tube formation assay. Red arrows denote VM channels formed by 143B cells. The results are expressed as the mean \pm SD of triplicate samples. Scale bars = 100 μ m. D): The *ITGA2*-knockdown 143B cells were injected intratibially into BALB/C nude mice. After 30 days, the mice and lungs were photographed. Red arrows denote 143B-injected limbs and white arrows denote metastatic nodules on the lung surface. E): Intratibial tumor volumes measured with calipers at the indicated time points. * $p < 0.05$, ** $p < 0.01$. F): *ITGA2* mRNA expression was detected in intratibial tumors from *ITGA2* KD group or NC group using qRT-PCR. G): The number of lung metastatic nodules in *ITGA2* KD group and NC group. H): Representative images of H&E and immunohistochemical staining of the resected tumor and lung from *ITGA2* KD group and NC group on day 30 post-inoculation. Black arrows denote micrometastatic tumors. Red arrows denote VM channels. I) Quantitative analysis of *ITGA2* staining. J): Quantification of VMD in *ITGA2* KD group and NC group. Scale bars = 50 μ m. The results are expressed as the mean \pm SD of eight samples. ** $p < 0.01$ compared to the NC group.

may contribute to VM formation. *MMP1* lists on the top of upregulated DEGs, consistent with previous findings demonstrating enhanced expression of *MMP1* in 143B cell which plays a central role in the development of pulmonary metastases in osteosarcomas [14]. *MMP14* have been implicated in VM formation in various carcinomas, making it potential target for anti-VM therapy [15]. Our result also showed that *MMP14* is upregulated by 3.18-fold in 143B group as compared to HOS group. But more impressingly, *MMP1* was upregulated much more dramatically than *MMP14* did in 143B group, implying the potential importance of *MMP1* in addition to *MMP14* for VM formation in osteosarcomas. *ITGA2* encodes a heterodimeric transmembrane receptor that mediates cell-ECM binding. Since interactions between tumor cells and their ECM-rich surroundings are necessary for VM, reports demonstrated that integrins like *ITGB1*,

ITGAV have been proven to participate in VM formation [16]. Increased *ITGA2* expression is also associated with increased osteosarcoma metastasis and invasion [17], suggesting its involvement in VM formation in osteosarcoma. *MYL9* lists on the top of downregulated DEGs. The decreased expression of *MYL9* represents stromal loss in tumor microenvironments [18], which could play a role in VM formation [2]. In this context, the impressive downregulation of *MYL9* in our finding may lead to an increased VM phenotype. Taken together, we hypothesized that these DEGs have the potential to be biomarkers for osteosarcoma VM.

GO categories like "collagen fibril organization," "calcium ion import" and "glycosaminoglycan biosynthetic process" was significantly upregulated in HOS compared to 143B groups, which is consistent with the fact that osteoblast-like HOS cells have an activity of bone formation [19]. Because

VM refer to the blood tubules formed by highly aggressive tumor cells, our finding of this non-metastatic, well-differentiated phenotype of HOS cells may explain why HOS were incapable of VM.

The increased expression level of “angiogenesis” and “positive regulation VEGF production” GO categories are in accordance with the enriched “VEGF signaling pathway” in 143B compared to HOS groups. Some pro-angiogenic molecules are crucial in tumor angiogenesis and equally have important function in VM formation [20]. In our results, *PTGS2* in the above-mentioned GO and pathway categories has fold change of 6.65. It is well known that *PTGS2* encodes a key enzyme COX-2 that generates PGE₂ that binds to prostanoid receptor and promotes tumor VM [21]. Additionally, COX-2 overexpression in osteosarcoma patients correlates with the occurrence of lung metastasis [22]. Based on the results of our study and others, we suggest that *PTGS2* might contribute to the development of VM in osteosarcoma.

“TGF-beta signaling pathway” was significantly upregulated in 143B compared to HOS groups, which is consistent with the GO category “regulation of TGF- β receptor signaling pathway” enriched in 143B. Bone morphogenic proteins (BMPs) constitute the largest member in TGF- β superfamily. BMPs are overexpressed in osteosarcoma and correlated with poor prognosis in bone tumors [23]. Study showed an important role of BMPs in supporting VM in metastatic tumor cell line [24]. Here, we demonstrated 4.74-fold change of *BMP6* in 143B compared with HOS, implying the possible involvement of *BMP6* in osteosarcoma VM.

GSEA pathway “Wnt signaling pathway” and GO “positive regulation of Wnt receptor signaling pathway” were upregulated in 143B group. Wnt signaling has been demonstrated to play an important role in VM in several studies [25]. Aberrantly activated Wnt pathway plays a key role in the development and metastasis of osteosarcoma and drugs targeting to inactivate this pathway are useful therapeutic application to inhibit osteosarcoma [26]. Thus, we can speculate that the significantly upregulated Wnt signaling pathway may facilitate osteosarcoma VM.

Signal-net analysis was performed to identify hub genes. *ITGA2*, listed as one of the top ten upregulated DEGs, also has the highest degree identified by signal-net analysis. The hub genes, which have many neighbors, are much more likely to be essential genes compared to non-hub genes. Thus, we herein focus our attention on the role of *ITGA2* in osteosarcoma VM. The loss-of-functional study demonstrated that knockdown of *ITGA2* lead to VM destruction both *in vitro* and *in vivo*, demonstrating the promoting role of *ITGA2* in VM formation. More importantly, VM functions as an alternative microcirculation to transmit blood fluid in tumor tissues and provide an escape route for new tumors in distant organs. Indeed, knockdown of *ITGA2* inhibited primary tumor growth as well as lung metastatic nodules in metastatic orthotopic-transplant mice model. These findings were consistent with previous studies that the expression of *ITGA2*

was associated with metastatic behaviors in osteosarcoma cells and other malignancies [27, 28]. *ITGA2* were involved in GO category “cell adhesion”. As mentioned before, integrins function as cell adhesion receptors for ECM proteins. Integrin-mediated cell adhesion activates a cytoplasmic protein tyrosine kinase called FAK, which has been recognized as a key factor in VM [28]. In our earlier findings, FAK was found to be activated in osteosarcoma VM [4]. We can speculate that *ITGA2* may promote VM formation of osteosarcoma by activating FAK signaling. Further studies are needed to explore this issue.

In conclusion, as far as we know, we showed for the first time the differential mRNAs expression profiles associated with VM phenotype in osteosarcoma cells. The enriched-GSEA GO terms and PATHWAY in 143B group indicated the possibility of their involvement in osteosarcoma VM formation. Furthermore, signal-net analysis identified key gene *ITGA2* with the highest degrees. Functionally, knockdown of *ITGA2* inhibited osteosarcoma VM formation as well as osteosarcoma growth and metastasis, suggesting its potential role in OS VM and metastasis. Given the crucial role of VM in poor prognosis for osteosarcoma, our datasets are expected to help elucidate the molecules engaged in osteosarcoma VM and determine potential targets for inhibiting metastasis of osteosarcoma.

Supplementary information is available in the online version of the paper.

Acknowledgments: This study was supported by the National Natural Science Foundation of China (No. 81903851, 81673017, 81572188, 21502014), the Jiangsu Province Natural Science Foundation (No. BK20191084, SBK2019040340, BK2012775), the Fundamental Research Funds for the Central Universities (No.2242016k40152), the Liaoning Province Natural Science Foundation (201602114) and the Research Foundation of Educational Committee of Liaoning Province (JDL2017027).

References

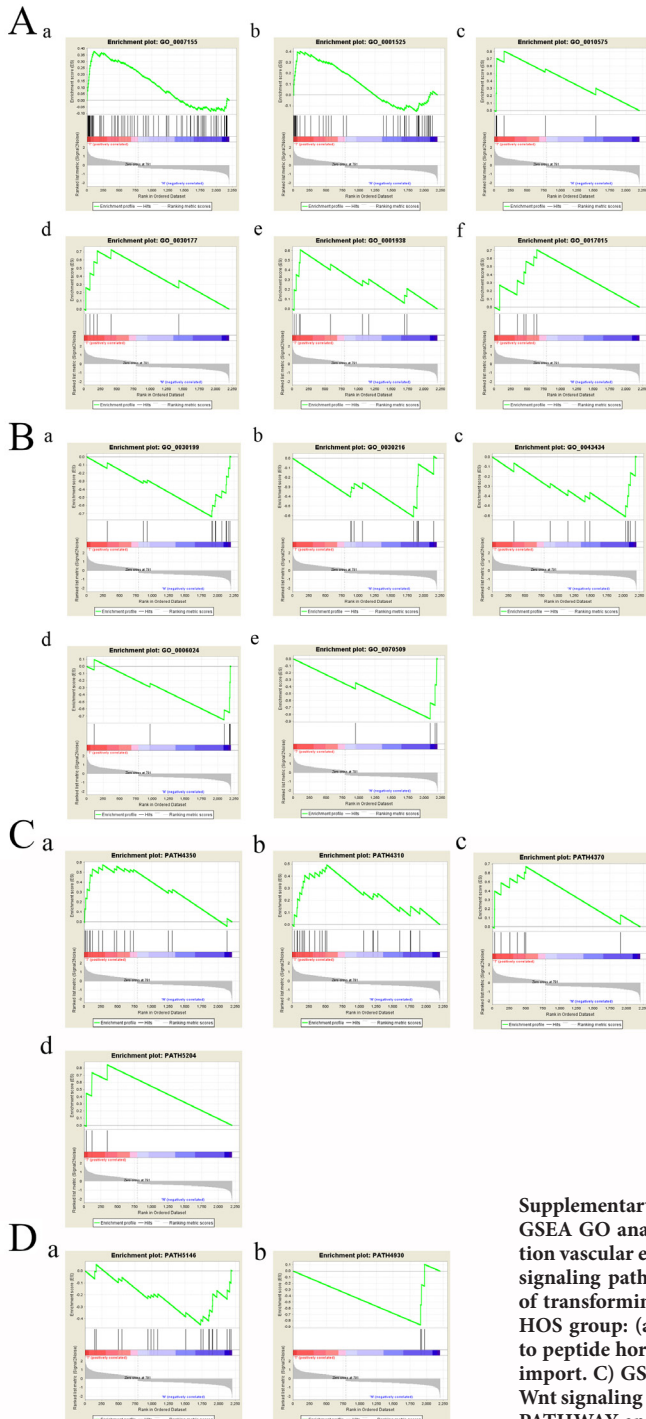
- [1] MANIOTIS AJ, FOLBERG R, HESS A, SEFTOR EA, GARDNER LM et al. Vascular channel formation by human melanoma cells in vivo and in vitro: vasculogenic mimicry. *Am J Pathol* 1999; 155: 739–752. [https://doi.org/10.1016/S0002-9440\(10\)65173-5](https://doi.org/10.1016/S0002-9440(10)65173-5)
- [2] HENDRIX MJ, SEFTOR EA, HESS AR, SEFTOR RE. Vasculogenic mimicry and tumour-cell plasticity: lessons from melanoma. *Nat Rev Cancer* 2003; 3: 411–421. <https://doi.org/10.1038/nrc1092>
- [3] FOLBERG R, ARBIEVA Z, MOSES J, HAYEE A, SANDAL T et al. Tumor cell plasticity in uveal melanoma: microenvironment directed dampening of the invasive and metastatic genotype and phenotype accompanies the generation of vasculogenic mimicry patterns. *Am J Pathol* 2006; 169: 1376–1389. <https://doi.org/10.2353/ajpath.2006.060223>

- [4] REN K, YAO N, WANG G, TIAN L, MA J et al. Vasculogenic mimicry: a new prognostic sign of human osteosarcoma. *Hum Pathol* 2014; 45: 2120–2129. <https://doi.org/10.1016/j.humpath.2014.06.013>
- [5] YAO N, REN K, WANG Y, JIN Q, LU X et al. Paris polyphylla Suppresses Proliferation and Vasculogenic Mimicry of Human Osteosarcoma Cells and Inhibits Tumor Growth In Vivo. *Am J Chin Med* 2017; 45: 575–598. <https://doi.org/10.1142/s0192415x17500343>
- [6] REN K, ZHANG J, GU X, WU S, SHI X et al. Migration-inducing gene-7 independently predicts poor prognosis of human osteosarcoma and is associated with vasculogenic mimicry. *Exp Cell Res* 2018; 369: 80–89. <https://doi.org/10.1016/j.yexcr.2018.05.008>
- [7] KIRSCHMANN DA, SEFTOR EA, HARDY KM, SEFTOR RE, HENDRIX MJ. Molecular pathways: vasculogenic mimicry in tumor cells: diagnostic and therapeutic implications. *Clin Cancer Res* 2012; 18: 2726–2732. <https://doi.org/10.1158/1078-0432.ccr-11-3237>
- [8] PAULIS YW, SOETEKOUW PM, VERHEUL HM, TJANHEIJNEN VC, GRIFFIOEN AW. Signalling pathways in vasculogenic mimicry. *Biochim Biophys Acta* 2010; 1806: 18–28. <https://doi.org/10.1016/j.bbcan.2010.01.001>
- [9] HENDRIX MJ, SEFTOR EA, SEFTOR RE, CHAO JT, CHIEN DS et al. Tumor cell vascular mimicry: Novel targeting opportunity in melanoma. *Pharmacol Ther* 2016; 159: 83–92. <https://doi.org/10.1016/j.pharmthera.2016.01.006>
- [10] BEHNSAWY HM, MIYAKE H, ABDALLA MA, SAYED MA, AHMED EFI et al. Expression of integrin proteins in non-muscle-invasive bladder cancer: significance of intravesical recurrence after transurethral resection. *BJU Int* 2011; 107: 240–246. <https://doi.org/10.1111/j.1464-410X.2010.09534.x>
- [11] ARNAOUTOVA I, KLEINMAN HK. In vitro angiogenesis: endothelial cell tube formation on gelled basement membrane extract. *Nat Protoc* 2010; 5: 628–635. <https://doi.org/10.1038/nprot.2010.6>
- [12] ANDO K, HEYMANN MF, STRESING V, MORI K, REDINI F et al. Current therapeutic strategies and novel approaches in osteosarcoma. *Cancers (Basel)* 2013; 5: 591–616. <https://doi.org/10.3390/cancers5020591>
- [13] MILLER BJ, CRAM P, LYNCH CF, BUCKWALTER JA. Risk factors for metastatic disease at presentation with osteosarcoma: an analysis of the SEER database. *J Bone Joint Surg Am* 2013; 95: e89. <https://doi.org/10.2106/jbjs.l.01189>
- [14] KIMURA R, ISHIKAWA C, ROKKAKU T, JANKNECHT R, MORI N. Phosphorylated c-Jun and Fra-1 induce matrix metalloproteinase-1 and thereby regulate invasion activity of 143B osteosarcoma cells. *Biochim Biophys Acta* 2011; 1813: 1543–1553. <https://doi.org/10.1016/j.bbamcr.2011.04.008>
- [15] SEFTOR RE, SEFTOR EA, KOSHIKAWA N, MELTZER PS, GARDNER LM et al. Cooperative interactions of laminin 5 gamma2 chain, matrix metalloproteinase-2, and membrane type-1-matrix/metalloproteinase are required for mimicry of embryonic vasculogenesis by aggressive melanoma. *Cancer Res* 2001; 61: 6322–6327.
- [16] RUFFINI F, GRAZIANI G, LEVATI L, TENTORI L, D'ATRI S et al. Cilengitide downmodulates invasiveness and vasculogenic mimicry of neuropilin 1 expressing melanoma cells through the inhibition of alphavbeta5 integrin. *Int J Cancer* 2015; 136: E545–558. <https://doi.org/10.1002/ijc.29252>
- [17] LIU X, LIANG Z, GAO K, LI H, ZHAO G et al. MicroRNA-128 inhibits EMT of human osteosarcoma cells by directly targeting integrin alpha2. *Tumour Biol* 2016; 37: 7951–7957. <https://doi.org/10.1007/s13277-015-4696-0>
- [18] HUANG YQ, HAN ZD, LIANG YX, LIN ZY, LING XH et al. Decreased expression of myosin light chain MYL9 in stroma predicts malignant progression and poor biochemical recurrence-free survival in prostate cancer. *Med Oncol* 2014; 31: 820. <https://doi.org/10.1007/s12032-013-0820-4>
- [19] TAKITOH T, KATO Y, NAKASU A, TADOKORO M, BESHOMO M et al. In vitro osteogenic differentiation of HOS cells on two types of collagen gels. *J Biosci Bioeng* 2010; 110: 471–478. <https://doi.org/10.1016/j.jbiosc.2010.04.009>
- [20] SMITH SJ, WARD JH, TAN C, GRUNDY RG, RAHMAN R. Endothelial-like malignant glioma cells in dynamic three dimensional culture identifies a role for VEGF and FGFR in a tumor-derived angiogenic response. *Oncotarget* 2015; 6: 22191–22205. <https://doi.org/10.18632/oncotarget.4339>
- [21] RONG X, HUANG B, QIU S, LI X, HE L et al. Tumor-associated macrophages induce vasculogenic mimicry of glioblastoma multiforme through cyclooxygenase-2 activation. *Oncotarget* 2016; 7: 83976–83986. <https://doi.org/10.18632/oncotarget.6930>
- [22] QU L, LIU B. Cyclooxygenase-2 promotes metastasis in osteosarcoma. *Cancer Cell Int* 2015; 15: 69. <https://doi.org/10.1186/s12935-015-0220-2>
- [23] MUNDY C, YANG E, TAKANO H, BILLINGS P, PACIFICI M. Heparan sulfate antagonist alters bone morphogenetic protein signaling and receptor dynamics, suggesting a mechanism in hereditary multiple exostoses. *J Biol Chem* 2018; 293: 7703–7716. <https://doi.org/10.1074/jbc.RA117.000264>
- [24] AZAD T, GHAREMANI M, YANG X. The Role of YAP and TAZ in Angiogenesis and Vascular Mimicry. *Cells* 2019; 8: E407. <https://doi.org/10.3390/cells8050407>
- [25] QI L, SONG W, LIU Z, ZHAO X, CAO W et al. Wnt3a Promotes the Vasculogenic Mimicry Formation of Colon Cancer via Wnt/beta-Catenin Signaling. *Int J Mol Sci* 2015; 16: 18564–18579. <https://doi.org/10.3390/ijms160818564>
- [26] YANG X, WANG L, WANG Q, LI L, FU Y et al. MiR-183 inhibits osteosarcoma cell growth and invasion by regulating LRP6-Wnt/beta-catenin signaling pathway. *Biochem Biophys Res Commun* 2018; 496: 1197–1203. <https://doi.org/10.1016/j.bbrc.2018.01.170>
- [27] CHUANG YC, WU HY, LIN YL, TZOU SC, CHUANG CH et al. Blockade of ITGA2 Induces Apoptosis and Inhibits Cell Migration in Gastric Cancer. *Biol Proced Online* 2018; 20: 10. <https://doi.org/10.1186/s12575-018-0073-x>
- [28] HESS AR, POSTOVIT LM, MARGARYAN NV, SEFTOR EA, SCHNEIDER GB et al. Focal adhesion kinase promotes the aggressive melanoma phenotype. *Cancer Res* 2005; 65: 9851–9860. <https://doi.org/10.1158/0008-5472.can-05-2172>

Identification of potential crucial genes associated with vasculogenic mimicry in human osteosarcoma based on gene expression profile

N. YAO^{1,2,#}, K. REN^{3,#}, X. J. GU⁴, S. J. WU⁵, X. SHI⁵, Q. CHANG³, Y.G. LI³, Z. X. GAO³, Q. M. JIN^{1,2}, J. ZHANG^{1,2}, C. WANG^{3,*}, J. ZHOU^{1,2,6*}

Supplementary Information



Supplementary Table S1. Primers used in qRT-PCR analysis.

Gene		Sequence (5'->3')
<i>MMP1</i>	Forward	GGCAAATCTGGCGTGTA
	Reverse	GGCTGAAAGTGACTGGGAAAC
<i>ITGA2</i>	Forward	TACCCAAGAAGTCTATGC
	Reverse	CGACGAAGTGCTACGAAA
<i>TRPA1</i>	Forward	CTACCAGAATAGGACGATA
	Reverse	ATAGACCCAGTGGAGAAG
<i>TBX15</i>	Forward	TCCAGTTCTGTTTCTCCC
	Reverse	ACCCACTAAGCCTGTTCC
<i>ANPEP</i>	Forward	TCTTCGTCGTAGTTCACCC
	Reverse	GCCCATCACATCCATCAG
<i>MYL9</i>	Forward	CATCTCGTCCACTTCCTCATC
	Reverse	AACGCCTTTGCCTGCTTC
<i>TNFRSF10D</i>	Forward	ACGATGAAGACGACGAAAC
	Reverse	GGGACGATTTCTGATTGA
<i>INA</i>	Forward	TCAGGTTGGCAAACCTGGACT
	Reverse	AGGTGGACGTGACTGTGGCT
<i>WSB1</i>	Forward	AACCCTGTAGCAAGAAGT
	Reverse	ATAAGCCTCGTGAACATA
<i>SRGN</i>	Forward	CCTGTTCCATTTCGGTTA
	Reverse	TGAATCGTATCTTCCCCTT
<i>PRKACB</i>	Forward	CTGAAGTGGGATGGGAAT
	Reverse	CAAGGGCTACAATAAGGC
<i>GJA1</i>	Forward	CCAGGAGGAGACATAGGC
	Reverse	TTCAAGGGCGTTAAGGAT
<i>PAK1</i>	Forward	GCATTCCCCTAAACTCCC
	Reverse	TTCTAAACCTCTGCCTCCAA
<i>FLNA</i>	Forward	CAATCAGGTAAACGCCATTC
	Reverse	TCAGGAGTCAGGGCTAAAGG
<i>GAPDH</i>	Forward	GGACCTGACCTGCCGTCTAG
	Reverse	GTAGCCCAGGATGCCCTTGA

Supplementary Figure S1. GSEA enrichment plots in 143B group and HOS group. A) GSEA GO analysis in 143B group: (a) cell adhesion (b) angiogenesis (c) positive regulation vascular endothelial growth factor production (d) positive regulation of Wnt receptor signaling pathway (e) positive regulation of endothelial cell proliferation (f) regulation of transforming growth factor beta receptor signaling pathway. B) GSEA GO analysis in HOS group: (a) collagen fibril organization (b) keratinocyte differentiation (c) response to peptide hormone stimulus (d) glycosaminoglycan biosynthetic process (e) calcium ion import. C) GSEA PATHWAY analysis in 143B group: (a) TGF-beta signaling pathway (b) Wnt signaling pathway (c) VEGF signaling pathway (d) Chemical carcinogenesis. D) GSEA PATHWAY analysis in HOS group: (a) Amoebiasis (b) Type II diabetes mellitus.